Bending strength of delaminated aerospace composites

By Moustafa Kinawy, Richard Butler and Giles W. Hunt

Composites Research Unit, Department of Mechanical Engineering, University of Bath, Bath, BA27AY, UK

Buckling-driven delamination is considered amongst the most critical failure modes in composite laminates. This paper examines the propagation of delaminations in a beam under pure bending. A pre-developed analytical model to predict the critical buckling moment of a thin sub-laminate is extended to account for propagation prediction, utilising mixed mode fracture analysis. Fractography analysis is performed to distinguish between Mode-I and Mode-II contributions to the final failure of specimens. Comparison between experimental results and analysis shows agreement to within 5% in static propagation moment for two different materials. It is concluded that static fracture is almost entirely driven by Mode-II effects. This result was unexpected since it arises from a buckling mode that opens the delamination. For this reason, and because of the excellent repeatability of the experiments, the method of test may be a promising means of establishing the critical value of Mode-II fracture toughness, G_{IIC} of the material. Fatigue testing on similar samples showed that buckled delamination resulted in a fatigue threshold that was over 80% lower than the static propagation moment. Such an outcome highlights the significance of predicting snap-buckling moment and subsequent propagation for design purposes.

Keywords: Buckling, delamination bending, fracture toughness, fatigue, mixed-mode

1. Introduction

Propagation of damage due to buckling of delaminations is one of the critical causes of failure in composite laminates. Such internal delaminations can originate from manufacturing defects or during service where low velocity impact damage can result in barely visible sub-layer delaminations. These may significantly decrease the load carrying capacity of the structure concerned.

Modelling of buckling-driven delaminations has been studied by many researchers. A good deal of work has investigated buckled delaminations under compressive loading. A one-dimensional mathematical model for delamination growth in a strut under compression was developed by Chai & Babcock (1981). They introduced a formula calculating the strain energy release rate in terms of buckling and propagation strains of a thin sub-laminate in the strut. Chai et al (1985) extended their previous model to incorporate parameters affecting delamination growth of two-dimensional delaminated plates under compression. An analytical model by Shan et al (2003a) accounted for forces and moments at the delamination tips when the local buckling of the sub-laminate interacted with global buckling of the specimen.

More recently, fatigue failure of composites has been predicted, following buckling of the thin sub-laminate created by delamination. Rhead et al (2008) concluded that when the applied compressive strain is sufficiently above the thin sub-laminate buckling strain level, the failure of a delaminated composite plate under compression occurs. They also gave an approximate, model-based method for predicting the fatigue strain level below which propagation would not occur. Their so-called Strip model was validated using experimental tests and nonlinear finite element analysis, Butler et al (2011).

Pure compression of structures in real loading scenarios is less frequent than bending induced compression. Delamination opening due to bending has been investigated. A low-dimensional model developed by Murphy & Nichols (2008) was introduced to obtain the critical moment at which buckling of a thin sub-laminate created by a delamination could occur within a cantilever beam under bending. Buckling due to pure bending was studied by Kardomateas (1990) who derived a formula for snap-buckling moment level at which delaminations instantaneously switch from closing to opening.

Curved composite beams with delamination were examined by Wang & Shenoi (2003), who developed an analytical model to study the propagation of a delamination placed near the outer surface under an opening moment. In their work, they concluded that the initial beam curvature and the arc angle of the delamination have significant effect on propagation. The delamination problem has also been covered in the analysis of micro electro mechanical systems (MEMS). Kosel et al (2005) presented a mathematical model predicting the level of axial force for delamination of the top layer of a two-layer plate. Their model included the elasto-plastic effect between the bonded layers. The model was solved numerically and verified by experimental testing. Shan & Pelgeri (2003b) introduced an analytical model of fracture behaviour for a cross-ply composite cantilever beam with an artificially embedded delamination. They also modelled the effect of loading asymmetry in the delamination contact zones by finite elements. They concluded that failure was dominated by Mode-II effects due to a large contact zone and that the deeper the delamination, the weaker the structure would become with respect to propagation. Kinawy et al (2011) gave a lower bound prediction of the critical moment for snap-buckling moment for a thin sub-laminate in a composite beam under pure bending. The model assumed isotropic material for both the sub-laminate and the base laminate. It also distinguished the bifurcation behaviour of the sub-laminate, which switches from a closing to an opening mode

This paper will investigate the post-buckling of a delaminated beam in bending and predict the moment at which the delamination propagates. A three degree-of-freedom Rayleigh Ritz model for post-buckling is used to determine the Mode I and II strain energy release rates, from which propagation is predicted. A comparison of the analytical model with experiments will be presented for propagation of unidirectional laminates constructed from two types of composite material. The results of a series of fatigue tests will also be presented.

2. Analytical Modelling

(*a*) *Post-buckling analysis*

Although the post-buckling analysis has been presented by Kinawy et al (2011), it is briefly described here because it forms the basis for subsequent propagation modelling. The model assumes that the beam is isotropic and the undelaminated end laminates are ignored in the prediction of the snap-buckling (or opening) moment, while the delaminated parts are modelled with bending and in-plane stiffness. Further assumptions are that rotation of the undelaminated region and each delaminated part is the same at their intersection, and that there is no friction between laminates at the interface. The end rotation forms one of the degrees of freedom Q_2. A second degree of freedom represents the end-shortening of the sub-laminates over the delaminated region. A further degree of freedom is used to describe the buckling displacement of the delaminated parts Q_1. Figure 1 shows a schematic of the delaminated beam and the applied moment. Note that positive Q_1 and negative Q_2 produce opening.

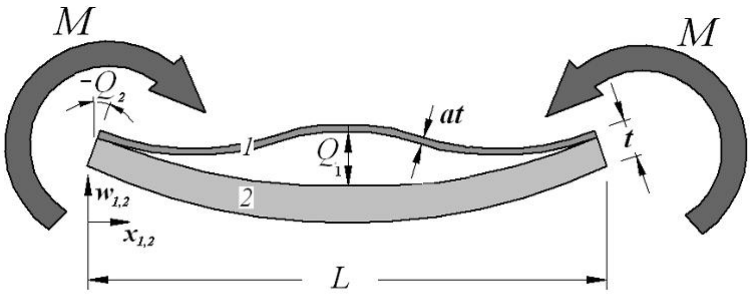

Figure 1. Delaminated beam coordinates and variables

The displacement functions for the delaminated and base parts are given as follows:

$$w_1(x) = Q_1 sin^2\big(\frac{\pi x_1}{L}\big) + Q_2\, x_1\big(\frac{L - x_1}{L}\big) \tag{2.1}$$

$$w_2(x) = Q_2 x_2\big(\frac{L - x_2}{L}\big) \tag{2.2}$$

The effect of initial imperfection was introduced to the model to investigate how the inclusion of an idealised PTFE layer used to create a delamination within the composite layers would affect snap-buckling. The imperfection is assumed to have a sine squared function of the form:

$$w_0(x) = Q_0 sin^2\big(\frac{\pi x_1}{L}\big) \tag{2.3}$$

In order to calculate the stretching energies in the system, the axial end shortening for the thin and thick sub-laminates is as follows:

$$\delta_1 = \Delta - \frac{1}{2}\int_0^L \left(\frac{d(w_1 - w_o)}{dx_1}\right)^2 dx_1 - Q_2(1-a)t \tag{2.4}$$

$$\delta_2 = \Delta - \frac{1}{2}\int_0^L \left(\frac{dw_2}{dx_2}\right)^2 dx_2 + Q_2 at \tag{2.5}$$

The strain energy of the system is obtained in terms of bending (U_B) and stretching (U_S) energy as follows:

$$U_B = \frac{EI_1}{2}\int_0^L \left(\frac{d^2(w_1 - w_o)}{dx_1^2}\right)^2 dx_1 + \frac{EI_2}{2}\int_0^L \left(\frac{d^2 w_2}{dx_2^2}\right)^2 dx_2 \tag{2.6}$$

$$U_S = \frac{t}{2L}\left(Ea\delta_1^2 + E(1-a)\delta_2^2\right) \tag{2.7}$$

The total potential energy of the system is:

$$V = U_B + U_S - 2MQ_2 \tag{2.8}$$

Substituting the displacement equations into the former equation leads to a potential function including three degrees of freedom in addition to the loading moment, $V(Q_1, Q_2, \Delta, M)$. By solving the partial equilibrium equation with respect to Δ, i.e: $\partial V(Q_1, Q_2, \Delta, M)/\partial\Delta = 0$ and substituting the resulting term into V, we obtain a two-degree of freedom term $V(Q_1, Q_2, M)$ i.e: $\partial V/\partial Q_1 = 0$, $\partial V/\partial Q_2 = 0$.

Solving the adapted system of equations as reported previously (Hunt et al 2004), the buckling displacement and rotation (Q_1, Q_2) are evaluated as functions of applied bending moment(M). The derivation process was carried out with mathematical manipulation software.

(*b*) *Propagation prediction using thin film analysis*

As the sub-laminate length to thickness ratio was approximately 80 for the example considered here, it can be approximated as an Euler strut which is compressed under bending. For predicting the propagation moment of the sub-laminate, a one dimensional mode by Chai et al (1981) was initially used. This model assumes that the ends of the thin sub-laminate do not rotate and calculates the critical strain energy release rate for the propagation of a compressed sub-laminate as follows:

$$G = \frac{Eat}{2}(\varepsilon - \varepsilon^C)(\varepsilon + 3\varepsilon^C) \tag{2.9}$$

The model ignores any bending energy that is released from the thick lower sub-laminate or from the end laminates. The buckling strain ε^C for the sub-laminate was calculated using the Euler formula for buckling of a strut fixed at each end, Equation (2.10), while the applied strain ε was formulated using Equation (2.11).

$$\varepsilon^C = \frac{\pi^2 a^2 t^2}{3L^2} \tag{2.10}$$

$$\varepsilon = \frac{6M(1-a)}{Et^2} \tag{2.11}$$

(c) *Mixed mode propagation*

Existence of curvature at the sub-laminate ends indicates that both Mode-I and Mode-II effects should be taken into consideration. The strain energy release rates G_I and G_{II} are calculated based on the stress intensities factors K_I and K_{II} near the delamination tips which using the approach taken by Hutchinson & Suo (1990) which assumed homogeneous isotropic layers and that force components are per unit width. The stress intensity factors are as follows:

$$K_I = \frac{P}{\sqrt{2atU}} cos\omega + \frac{M^*}{\sqrt{2a^3t^3V}} sin(\omega+\gamma) \tag{2.12}$$

$$K_{II} = \frac{P}{\sqrt{2atU}} sin\omega - \frac{M^*}{\sqrt{2a^3t^3V}} cos(\omega+\gamma) \tag{2.13}$$

where P and M^* are the linear combinations of the applied force P_1 and moments M and M_1 at the delamination edges shown in Figure 2.

$$P = P_1 - \frac{CM}{\eta t} \quad , \qquad M^* = M_1 - C^* M$$

and the geometric factors are:

$$C = \frac{6/\eta}{(1/\eta+1)^3} \quad , \quad C^* = \frac{1}{(1/\eta+1)^3} \quad , \quad \eta = \frac{a}{1-a}$$

$$\frac{1}{U} = 1 + 4\eta + 6\eta^2 + 3\eta^3 \quad , \quad \frac{1}{V} = 12(1+\eta^3)$$

γ and ω are obtained through:

$$\omega = 52.1^o - 3^o\eta \quad , \quad sin\gamma = 6\eta^2(1+\eta)\sqrt{UV}$$

From which the following strain energy release rates are obtained:

$$G_I = \frac{K_I^2}{2E} \qquad , \qquad G_{II} = \frac{K_{II}^2}{2E} \tag{2.14}$$

where E is the effective longitudinal modulus for the layer material. The division by two in Equation (2.14) is added assuming that propagation occurs at both delamination fronts simultaneously as a result of symmetry.

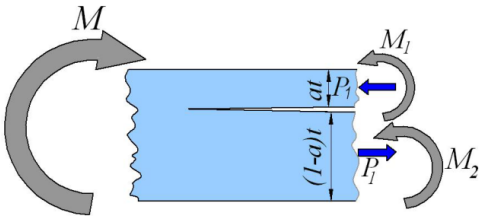

Figure 2. Force and moment components at delamination edge.

In order to obtain the strain energy release rates in Equation (2.13) the force P_1 and moment M_1 at the left end of the thin sub-laminate are required. The thin sub-laminate is assumed to carry only the critical buckling load, i.e:

$$P_1 = \varepsilon^C Eat \tag{2.15}$$

Where ε^C is derived using Equation (2.10). M_1 is calculated from the curvature of the thin sub-laminate, obtained by evaluating the second derivative of Equation (2.1) at $x_1 = 0$.

3. Experimental Setup and Methodology

Static tests were performed on specimens made from two different materials to understand their buckling and propagation behaviour. Specimens with 4 mm nominal thickness were manufactured from a 16 ply unidirectional T800/M21 and a 32-ply unidirectional IM7/8552. In order to form a through-width delamination, a PTFE (polytetrafluoroethylene) layer of 0.02 mm thickness was placed at the mid-length of each plate at a depth of thickness ratio $a = 0.125$, i.e. between the second and third ply for the T800/M21 plate and between the fourth and fifth ply for the IM7/8552 plate. The delamination length in both arrangements was 40 mm. The plates were laid up, bagged and then cured using an autoclave. The cured plates were cut into specimens with dimensions of (220 x W x t mm) where W and t are given in Tables 1 and 2. Each specimen had two strain gauges positioned on the centre of the top and bottom surfaces to measure the strain at which buckling of the sub-laminate occurred. An INSTRON-1332 servo-hydraulic machine with 10kN load cell was used for loading application. The strain gauges and loading channel from the servo-hydraulic machine were connected to a SPIDER-8 data acquisition system which was attached to a PC. The specimens were then loaded through the four point bending fixture shown in Figure 3 under displacement control. The fixture had movable supports to adjust the inter distances and a pivot to ensure uniform bending load application. The centre of delaminations was positioned at the centre of the fixture upper and lower parts.

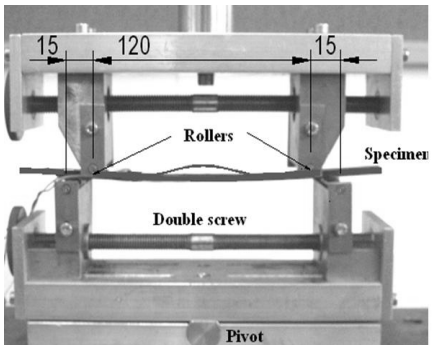

Figure 3. Four point bending test fixture showing specimen with delamination open (loaded above snap-buckling moment). Dimensions in mm.

4. Experimental Results

Strain gauges were used to observe the change in strain value on top and bottom surfaces of the specimen, where a sudden change of the top strain gauge indicated buckling of the sub-laminate. The slopes of both gauge lines were shown to be linear up to snap-buckling. The change in strain was found to occur suddenly in some specimens and with small smooth transition in others. The snap-buckling moment was taken as the moment at which the surface strain switched from compression to tension. Tables 1 and 2 show snap-buckling moment values for different tested specimens manufactured from both materials. In Table 1, it was shown that the moment values for the snap-buckling had an average value of 270 Nm/m for T800/M21 specimens, while one test showed a higher moment value of 668 Nm/m (presented in Table 1). The average measured strain on the compression surface at buckling was around 510 microstrain. Table 2 presents an average snap-buckling moment of 217 Nm/m for IM7/8552 specimens. The sub-laminate buckling mode tended to have the form of a clamped-clamped buckling mode in both specimen sets.

(*a*) *Propagation moment results*

Whilst increasing the load, the strain gauges failed to give any reading above a strain level of about 6000 microstrain. Hence, in order to observe the moment value at which propagation occurred, the load versus actuator displacement plot was acquired. Figure 4 shows a plot for one of the T800/M21 specimens. Propagation occurred as displacement increased while load was constant. Simultaneous delamination growth at both ends was observed during this region until the specimen reached its full failure. The propagation moment values for both specimen sets are shown in Tables 1 and 2. The average propagation moment values were 2725 Nm/m and 2254 Nm/m for T800/M21 and IM7/8552 specimens, respectively.

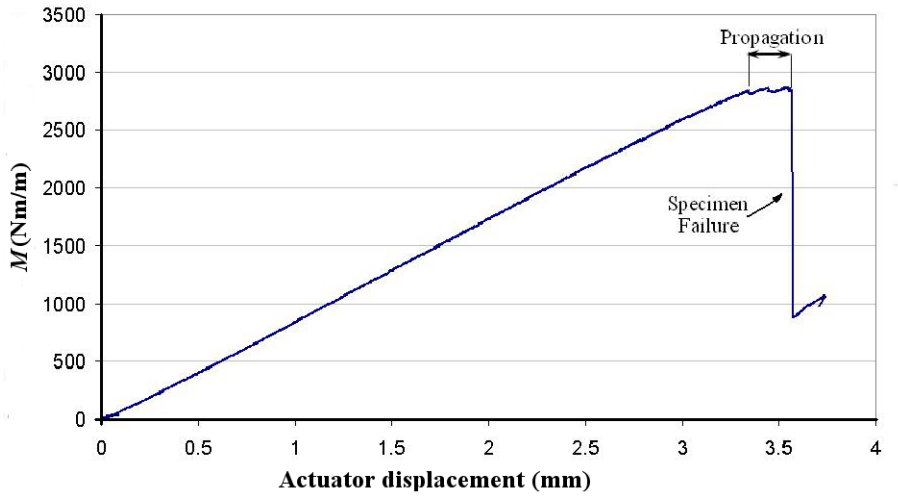

Figure 4. Applied moment versus displacement for T800/M21 specimen

Table 1. *Static test results for T800/M21 specimens*

Test No.	Width W(mm)	thickness t(mm)	Snap-buckling moment(Nm/m)	Propagation moment(Nm/m)
1	8.38	4.22	668	2779
2	8.41	4.31	273	2645
3	8.14	4.17	247	2824
4	9.15	4.22	273	2573
5	10.98	4.27	267	2675
6	10.78	4.30	320	2853
7	10.95	4.24	298	-
8	10.94	4.33	261	-
9	11.00	4.22	221	-
Avg.	10.27	4.25	270	2725
C.V.%	1	1	12	4

Table 2. *Static test results for IM7/8552 specimens*

Test No.	Width W(mm)	thickness t(mm)	Snap-buckling moment (Nm/m)	Propagation moment (Nm/m)
1	10.40	3.96	152	2200
2	10.34	3.97	221	2300
3	10.18	3.99	287	2300
4	10.25	3.97	283	2150
5	10.24	3.96	184	2344
6	10.20	3.95	176	2230
Avg.	10.27	3.97	217	2254
C.V.%	1	1	30	3

(*b*) *Electron scanning microscopy*

The images in Figure 5 show ESM scans of two specimens made of the T800/M21 material system. Images in Figures 5-a and 5-b are for a specimen tested in pure Mode-I conditions using the Double Cantilever Beam (DCB) test, according to ASTM D-5528. The images show the damage propagated in the resin rich areas and as the distance from the crack edges increases, the proportion of resin damage decreases and the damage was dominated by fibre bridging (Greenhalgh, 2009). Figures 5-c and 5-d show images obtained for one of the through-width centred-delamination specimens tested under four point bending as described above. Such loading allowed the top delaminated layer to buckle and then to propagate as the load advanced. The image of Figure 5-c shows that damage was dominated by shear cusps which characterise failure for Mode-II fracture (Greenhalgh, 2009). The cusps are distributed within the resin area with valleys perpendicular to the fibre direction. Figure 5-d, taken around 20 mm away from the delamination front, shows that the proportion of fractured zones is similar to that near the delamination front. This suggests that the delamination is also dominated by Mode-II fracture away from the delamination front due to the large contact area at this front.

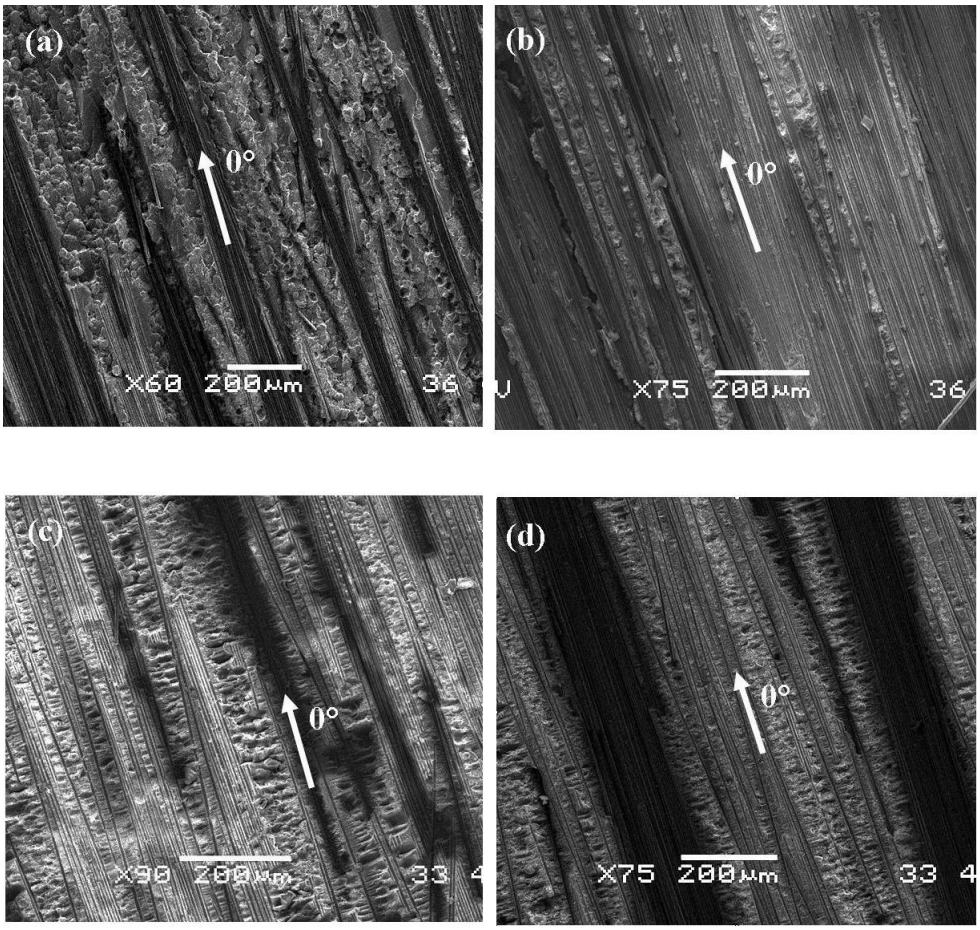

Figure 5. ESM images of fracture surfaces for T800/M21 material. a) DCB specimen near delamination front. b) DCB specimen 20 mm away from delamination front. c) Four-point bending specimen near delamination front. d) Four-point bending specimen 20 mm away from delamination front. In all cases, the fibre direction is shown.

5. Fatigue test results

In order to study the fatigue strength, a series of fatigue tests were performed under four point bending. A varying pure bending moment was applied to investigate the delamination growth. The loading moment was applied so that the sub-laminate was kept under compression throughout the fatigue cycle. The loading ratio R is defined as the ratio between the maximum to minimum applied moment within the cycle. For all tests the loading ratio was kept at R=10 with a test frequency of 4 Hz. The severity is calculated as the ratio between the maximum applied moment during the cycle to the average propagation moment from the static tests for both material specimens. Specimens were tested under loading control. The loading severity ranged from 0.85 to 0.17 so that a part of the loading cycle always passed through the average critical snap-buckling moment value observed in static tests. The tested specimens had similar dimensions to those tested under static

loading with their sides marked with 1 mm gratings around the delamination ends in order to monitor the total delamination extension during testing. They were loaded by the four point bend fixture shown in Figure 3. The tests were stopped after 10^6 cycles or if specimen failure occurred. Figures 6 and 7 represent the delamination extension versus number of cycles for different severities of load applied to specimens made from the two materials. The delamination growth decreased as the severity level decreased until reaching no delamination growth at a severity level of 0.1725 and 0.175 after 10^6 cycles for the T800/M21 and IM7/8552 materials, respectively.

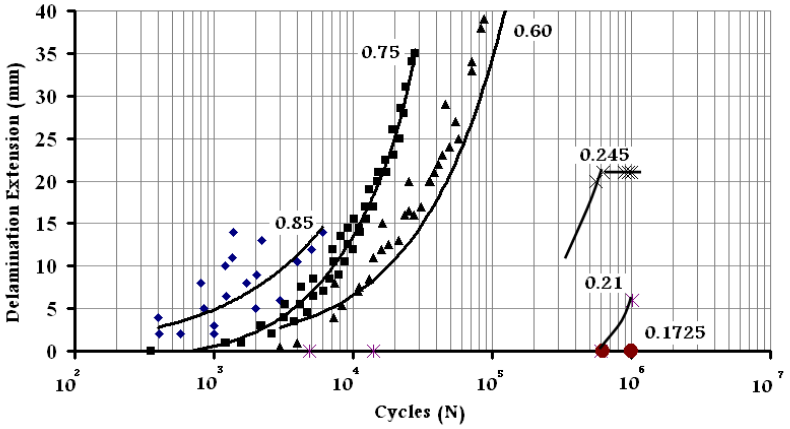

Figure 6. Delamination extension versus number of cycles for T800/M21 specimens at a range of severities. (Note, severity level of 1.0 indicates maximum value of moment =2725 Nm/m.)

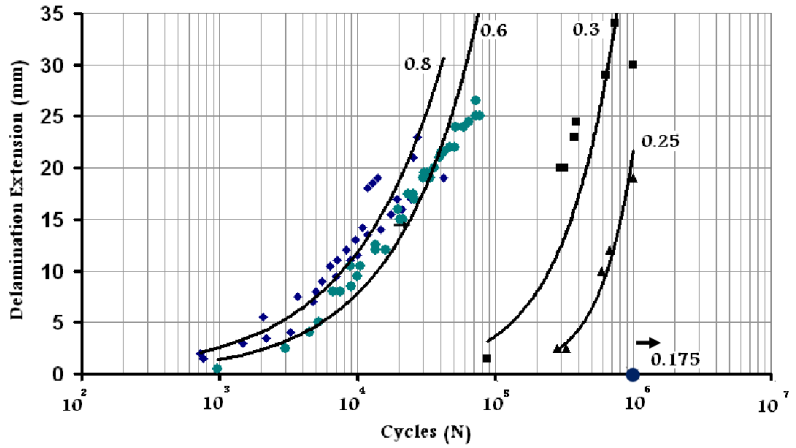

Figure 7. Delamination extension versus number of cycles for IM7/8552 specimens at a range of severities. (Note, severity level of 1.0 indicates maximum value of moment =2254 Nm/m.)

6. Analytical model results

The model was verified through three steps: first to check the snap-buckling moment level, second to check the kinematics during the post-buckling process and finally to check the propagation moment value. For the sake of verification, the two delaminated beam specimens described above were analysed. The first set was manufactured from 16 layers of unidirectional T800/M21 carbon fibre prepreg while the second was from 32 layers of unidirectional IM7/8552 carbon prepreg. Mechanical properties for each material system are included in Table 3.

(*a*) *Snap-buckling moment*

By minimising the energy of Equation (2.8) with respect to Q_1 and Q_2, the snap-buckling amplitude Q_1 and end rotation Q_2 are obtained as functions of the applied bending moment M. The system of equations was solved for both material systems assuming an initial imperfection value Q_o=0.02 mm in Equation(2.3). Average moduli and cured ply thicknesses (Table 3) were used as the model assumes the material to be isotropic. The resulting solution of Q_1 for the T800/M21 beam configuration is shown in Figure 8. Note that the infeasible solution (negative side) corresponds to the thin and thick sub-laminates passing through each other.

As seen in Figure 8, the critical moment for the equilibrium solution does not appear as a distinct point on the moment vs. Q_1 plot. The critical moment for an unstable system is characterised by more rapid growth of the deflections as the critical moment of the perfect system is approached (Thompson & Hunt, 1973). In order to obtain this point, a parametric study was carried out on the system of equations by changing the initial imperfection value (Q_o) to produce the convergence trend of the resulting (Q_1) plots (see Figure 8). For the aforementioned delaminated beam system, the imperfection was changed from 0.02 mm to 0.07 mm which showed that the critical moment level converged around a value of 300 Nm/m for T800/M21 specimen configuration. Running similar analysis, a value of 230 Nm/m was obtained for snap-buckling of the IM7/8552 specimen configuration. Note that, in reality the tests contained varying amount of geometric imperfection and manufacturing defects, hence the scatter in snap-buckling moments in Tables 1 and 2.

Table 3. *Mechanical properties for T800/M21 and IM7/8552 carbon prepregs*

Material	E_{11} (GPa)	G_{IC} (J/m^2)	G_{IIC} (J/m^2)	Cured Ply thickness (mm)
T800/M21	139	550	1400	0.260
IM7/8552	161	210	1000	0.123

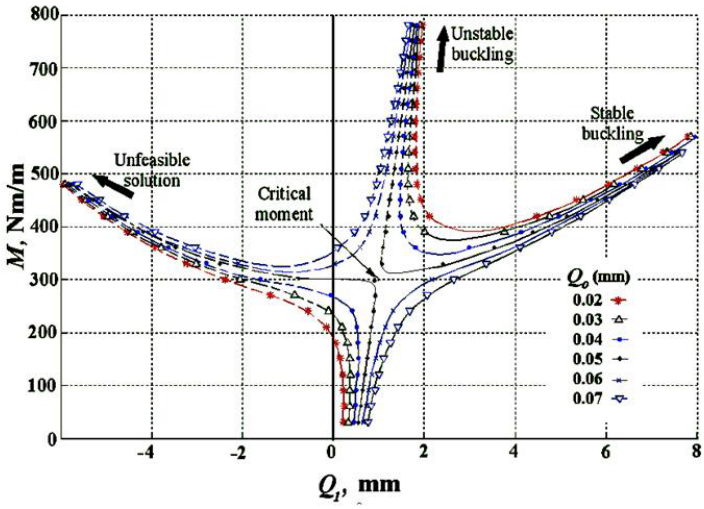

Figure 8. Equilibrium solutions showing analytical displacement Q_1 against applied moment per unit width M for a range of imperfections Q_o (T800/M21 specimen)

.

(*b*) *Kinematic results*

The kinematics of the model are important in order to obtain the force and moment components at the delaminated fronts. Such components were used to calculate the strain energy release rate at propagation. This was performed by measuring the out-of-plane displacement (Q_1) experimentally and comparing it against the analytical value. A high resolution camera was used to take snap-shots centred and focused on one side of the specimen at different loads. Each image was then enlarged to its maximum resolution capacity to reduce the measuring error. Finally, vector image manipulation software was used to measure the required value. The opening displacement (Q_1) was measured between the innermost edges of the upper and lower sub-laminates and then compared to the total thickness of the specimen at a marked place which was initially measured using a digital vernier. Figures 9-a and 9-b show graphical comparisons between experimentally acquired values for opening displacement (Q_1) and the predicted values by the model. There is good agreement between the experiment and model for both the T800/M21 and the IM7/8552 material specimens.

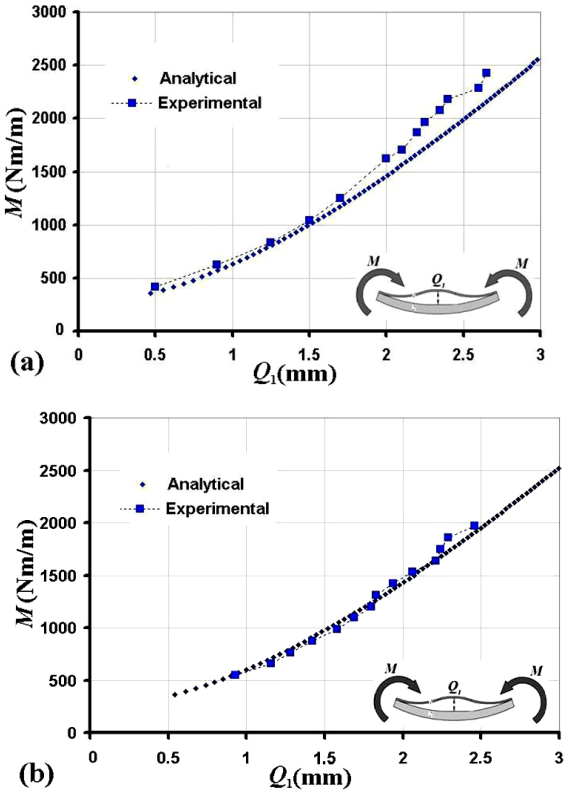

Figure 9. Out-of-plane displacement Q_1 comparison for a) T800/M21 specimen, b) IM7/8552 specimen. In both analyses, Q_o=0.02 mm.

(*c*) *Propagation moment*

After investigating the model kinematics, the post-buckling results of the analytical model were used to predict the propagation moment using two analytical methods. The first method was based on thin film analysis (Chai *et al.* , 1981). As an initial approximation, Mode-I critical values of G_{IC} for T800/M21 and IM7/8552 configurations were substituted in Equation (2.9), then equations (2.10) and (2.11) were used to calculate moment levels for propagation. They were found to be 1430 Nm/m and 850 Nm/m for T800/M21 and IM7/8552, respectively which are significantly less than the average value from static tests results. Such a comparison suggests that Mode-II has more influence upon propagation than Mode-I, and so two mixed mode analysis is considered next.

The second analytical method was based on the assumption of an isotropic material. The key material properties for predicting the propagation using the latter method were axial modulus, critical fracture toughness for Mode-I, critical fracture toughness for Mode-II. The model calculates the Mode-I and Mode-II energy components using the moment and force values at the delaminated edge as described through equations (2.12)-(2.14). Such values were calculated from the post-buckling analysis. The values of Q_1 and Q_2 were extracted for the stable branch of the equilibrium diagram in Figure 8 by minimising the energy of Equation (2.8). Strain

energy release rate for Mode-I and Mode-II components (G_I and G_{II}) were evaluated using Equation (2.14).

The critical Mode-II toughness value G_{IIC} is generally thought to be an unpredictable material property. So, it was checked against results obtained elsewhere for the M21 resin and found to range from 1200 J/m^2 (Zitoune & Collombet, 2007) to 1600 J/m^2 (Bouvet *et al.* , 2010). For analysis of T800/M21 specimens, the critical value for G_{IIC} was taken as 1400 J/m^2 similar to a characterisation test by Ilias(2010). Fracture toughness values, G_{IC} and G_{IIC}, for IM7/8552 material were assumed to be 210 J/m^2 and 1000 J/m^2 respectively (May & Hallett, 2010). The failure index (G_I/G_{IC}+G_{II}/G_{IIC}) was calculated for specimens made from both material configurations.

Figure 10 shows a plot for the strain rate release rate for the T800/M21 specimen. Using the material properties stated in Table 3, a failure index of 1.0 corresponds to a moment value of 2627 Nm/m which is 3.6% below the average propagation moment recorded in experiments. It is observed that, by increasing the applied moment, the curvature increased and the Mode-I component approached zero while Mode-II was dominant for inducing propagation. A similar conclusion was reached by Shan & Pelgeri (2003b), that Mode-II fracture dominates when the contact zone of delaminated beams increases due to beam curvature. For the IM7/8552 specimen configuration, Figure 11 shows the predicted propagation moment when is predicted at 2150 Nm/m which is 2% less than the observed propagation moment in experiments.

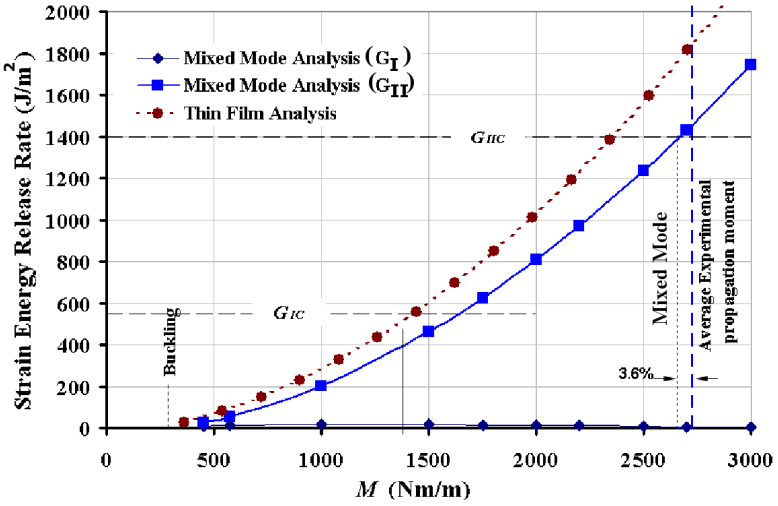

Figure 10. Strain energy release rate using the thin film and mixed-mode analysis for the delaminated, post-buckled beam - T800/M21 specimens.

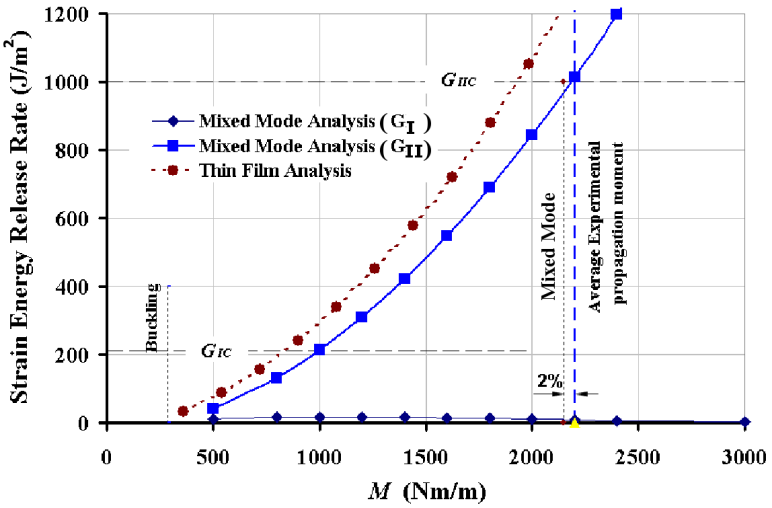

Figure 11. Strain energy release rate using the thin film and mixed-mode analysis for the delaminated, post-buckled beam - IM7/8552 specimens.

7. Discussion of Results

Static test experiments performed on T800/M21 specimens showed an average snap-buckling moment value of 270 Nm/m which is 11% less than the value obtained using *Rayleigh-Ritz* methodology. While experiments on IM7/8552 specimen showed a value of 217 Nm/m which is 9% less than the model. The analysis included the effect of an initial imperfection on the buckling moment value. The solution of the system revealed three equilibrium branches (see Figure 8): infeasible, unstable and stable, where the infeasible branch means the sub-laminates pass through one another. One tested T800/M21 specimen with snap-buckling moment value of 668 Nm/m seemed to follow the unstable branch until it snapped onto the stable (opening) branch of the plot. Other specimens followed the stable branch of the plot throughout.

Electron scanning microscopy of a failed T800/M21 specimen tested under bending showed a repeated pattern of shear cusps. The axes along the cusps valleys were perpendicular to fibre direction. The cusps occupied a similar area when the scan was repeated at 20 mm away from the delamination front. Such observation suggests that Mode-II contribution was significant as the delamination propagated at the bent fronts of the delamination. Scanning images for a failed DCB specimen made of the same material showed a typical textured area caused by plastic peeling of resin rich areas, which characterises pure Mode-I failure of tough resin material. Rothschild et al (1988) suggested the dominating effect of Mode-II over Mode-I at the delamination front for beams bent as a result of compression. They studied thin film delamination under compression, and showed that the delamination geometry is not symmetric about the delamination front; hence the opening moment for the top delaminated layer gives rise to interlaminar shear stresses at the delamination tip. This increases Mode-II significantly more than Mode-I. Such an effect may be similar to the case presented in this study as the bending of the beam

induces opening of the top delaminated layer. The comparison of modelled out-of-plane displacement Q_1 showed excellent agreement with measured values in both T800/M21 and IM7/8552 configurations (see Figures 9-a and 9-b). The derived propagation model analyses were used to predict the propagation moment levels for the T800/M21 and IM7/8552 specimens.

Thin-film analysis showed a significant deviation from experimentally acquired propagation moments when only incorporating Mode-I fracture toughness value within the model. Incorporating the total dissipated energy release rate ($G_{IC} + G_{IIC}$) would lead to closer predicted values for both material configurations, see Figures 10 and 11. Such approximation may be valid for the current problem as the thin sub-laminate has a high ratio between length and cross sectional dimensions. This suggests that Euler strut relations can be used. But for shorter lengths, thin film analysis may not be recommended.

The mixed mode analysis was investigated. It includes two different expressions for Mode-I and Mode-II fracture toughness energies G_I and G_{II}. Both energy terms depend on the force and moment components at the delamination edge. A failure index ($G_I/G_{IC} + G_{II}/G_{IIC}$) was used to predict the propagation moment level. While Mode-I fracture toughness G_{IC} was of small influence, G_{IIC} was a key parameter in the analysis and the predicted propagation moment value. Consequently, utilising power-based failure indices such as $(G_I/G_{IC})^2 + (G_{II}/G_{IIC})^2$, the propagation results will not significantly differ from the results obtained using the current failure index.

The experimentally determined value of Mode-II fracture toughness, G_{IIC}, is known to vary between tests in fibre epoxy materials, so the G_{IIC} values for the two materials were checked against different values found in the literature to be in the region of 1400 J/m^2 and 1000 J/m^2 for T800/M21 and IM7/8552 specimens, respectively. By incorporating a mixed mode strategy developed by Hutchinson & Suo(1992) for the example considered above, Mode-I had a similar influence to Mode-II immediately after the snap-buckling moment level. The Mode-I contribution then diminishes as the load increased. Finally, the propagation failure was dominated by Mode-II due to the increase in curvature of the beam during bending, which gives rise to shear stress at the contact surface. The deviation between analytical prediction and experiments was 3.6% and 2% for T800/M21 and IM7/8552 configurations, respectively.

Fatigue tests were performed on both specimen types using the same static test configurations. No fatigue growth was observed when the applied moment was 80% below the static strength value in both cases. Fatigue growth of the delamination occurred after 10^6 cycles at a moment that was 75% above the snap-buckling moment. This is a lower moment than might be expected considering that static propagation did not occur until about 10 times the snap-buckling moment.

8. Conclusions and future work

Delaminated beams made from unidirectional carbon fibre composites were studied under pure bending moment. A nonlinear mathematical model was used to predict the moment level for snap-buckling of the upper sub-laminate while including the effect of the initial imperfection created by the PTFE used to delaminate the beam. The method showed two types of sub-laminate behaviour; opening (stable)

and closing (unstable). The predicted moment levels for snap-buckling were 11% and 9% less than an average experimental value for unidirectional T800/M21 and IM7/8552 beams respectively. A mixed mode technique (Hutchinson & Suo, 1992) was applied and the propagation moment was found to be approximately 3.6% and 2% compared to experimentally obtained values for the T800/M21 and IM7/8552 beams respectively. As observed by electron scanning microscopy, Mode-II failure characterised the bend T800/M21 beams in question compared with a previous DCB test specimen failure which is a pure Mode-I failure. A similar outcome was predicted by the model which suggested that Mode-II has more influence than Mode-I behaviour in static propagation.

One interesting outcome of the current combined analytical technique is that it represents a promising method to determine Mode-II fracture toughness property, since tested specimens showed propagation in a repeatable manner for both types of material systems. Such repeatability is not the case for G_{IIC} values obtained by typical Mode-II characterising tests such as End Notched Flexure (ENF) and Four-Point Notched Flexure (4ENF) . Consequently, by applying the mixed-mode methodology along with the obtained propagation moment results from experiments, G_{IIC} values of 1480 (J/m^2) and 1030 (J/m^2) would correspond to T800/M21 and IM7/8552 material systems respectively.

Fatigue tests showed that crack growth occurred at a comparatively low level of severity (around 20% of the static propagation moment) before one million cycles, which highlights the importance of predicting the likelihood of an opening mode for a near-surface delamination. Such a low growth level might be due to the geometry of the tested beam, i.e. it had a near-surface through-width delamination. In real applications, damage usually consists of enclosed delaminations distributed within the thickness of the laminate. However, the result underlines the weakness of composites when subject to moments causing delamination opening.

For future work, specimens containing circular delamination should be tested in both static and fatigue loading to check for applicability of the analytical methods used in this study.

The authors would like to acknowledge Rolls-Royce and Agusta-Westland for their funding and support of the work.

References

Bouvet, C., Rivallant, S., & Barrau, July 2010. Modelling of impact damage and permanent indentation on laminate composite plate. *In: 14th European Conference on Composite Materials (ECCM-14), Budapest, Hungary.*

Britvek, S.J. 1973. *The stability of elastic systems.* Pergamon, New York.

Butler, R., Rhead, A.,T., Liu, W., Kontis, N., 2011. Compressive strength of delaminated aerospace composites. *Philosophical Transactions-A, Royal Society*, In review.

Chai, H., & Babcock, C.D. 1985. Two-dimensional modelling of compressive failure in delaminated laminates. *Journal of Composite Materials*, **19**, 67–98.

Chai, H., Babcock, C.D., & Knauss, W. 1981. One dimensional modelling of failure in laminated plates by delamination buckling. *International Journal of Solids and Structures*, **17**, 1069–1083.

Greenhalgh, E.S. 2009. *Failure analysis and fractography of polymer composites.* Woodhead Publishing Limited, Cambridge, UK.

Hutchinson, J. W., & Suo, Z. 1992. Mixed mode cracking in layered materials. *Pages 63–191, Advances in Applied Mechanics*, vol. 29, Academic Press.

Ilyas, M. 2010. *Damage modeling of carbon/epoxy laminated composites submitted to impact loading.* Ph.D. thesis, L'Universite de Toulouse.

Ilyas, M., Lachaudl, F., Espinosa, Ch., & Salan, M. July 2009. Dynamic delamination of aeronautic structural composites by using cohesive finite elements. *In: 17th International Conference on Composite Materials (ICCM- 17), Edinburgh, Scotland.*

Kardomateas, G.A. 1990. Snap buckling of delaminated composites under pure bending. *Journal of Composites Science and Technology*, **39**, 63–74.

Kinawy, M., Butler, R., & Hunt, G.W. 2011. Buckling and postbuckling of a delaminated composite beam in bending. *AIAA Journal , doi: 10.2514/1.j050784- in press.*

Kosel, F., Petrisic, J., Kuselj, B., Kosel, T., & Sajn, V., Brojan M. 2005. Local buckling and debonding problem of a bonded two-layer plate. *Journal of Applied Mechanics*, **74**, 704-726.

May, M., & Hallett, S.R. 2010. A combined model for initiation and propagation of damage under fatigue loading for cohesive interface elements. *Composites part A: Applied Science and Manufacturing, doi:10.1016/j.compositesa.2010.08.015- in press.*

Murphy, K.D., & Nichols, J.M. 2008. A low-dimensional model for delamination in composite structures: Theory and experiment. *International Journal of Nonlinear Mechanics*, **45**, 13–18.

Rhead, A., Butler, R., & Hunt, G.W. 2008. Post-buckled propagation model for compressive fatigue of impact damaged laminates. *International Journal of Solids and Structures*, **38**, 4349–4361.

Rothschilds, R.J., Gillespie, J.W., & Carlsson, L.A. 1988. Instability-related delamination growth in thermoset and thermo-plastic composites. *In:* Whitcomb, J. D. (ed), *Proceeding of Composite Materials: Testing and Design Conference, ASTM STP 972.*

Shan, B., & Pelegri, A. 2003a. Approximate analysis of the buckling behavior of composites with delamination. *Journal of Composites Materials*, **37**, 673–685.

Shan, B., & Pelegri, A. 2003b. Assessment of the fracture behavior of an asymmetrically loaded cantilever composite structure. *Journal of Engineering Materials and Technology*, **125**, 353–360.

Thompson, J.M., & Hunt, G.W. 1973. A general theory of elastic stability. Wiley-Interscience, London and New York.

Wang, W., & Shenoi, R.A. 2003. Delamination modelling of a curved composite beam subjected to an opening bending moment. *Journal of Strain Analysis*, **38**(5), 453–457.

Williams, J.G. 1993. A review of the determination of energy release rates for strips in tension and bending: Part I - static solution. *Journal of Strain Analysis*, **28**(4).

Zitoune, R., & Collombet, F. 2007. Numerical prediction of the thrust force responsible of delamination during the drilling of the long-fibre composite structures. *Composites-A: Applied Science and Manufacturing*, **38**(3), 858 – 866.